BC RESEARCH ARTICLE



The deacetylase NagA mediates the remodeling and recycling of peptidoglycan-derived amino sugars in mycobacteria

Received for publication, March 13, 2025, and in revised form, July 7, 2025 Published, Papers in Press, August 14, 2025 https://doi.org/10.1016/j.jbc.2025.110597

Collette S. Guy¹, Charlotte Cooper^{1,‡}, Magdalena Karlikowska^{1,‡}, James Harrison¹, Albel Singh², Luis Steven Servín-González 0, Caroline A. Evans 0, Saskia E. Bakker 0, Andrew Bottrill 0, Apoorva Bhatt, Stéphane Mesnage (0, Gurdyal S. Besra 0, and Elizabeth Fullam 1,5,6,* 0

From the ¹School of Life Sciences, University of Warwick, Coventry, UK; ² Institute of Microbiology & Infection, School of Biosciences, University of Birmingham, Birmingham, UK; ³Department of Chemical and Biological Engineering, ChELSI Institute, and ⁴School of Biosciences, University of Sheffield, Sheffield, UK; ⁵Manchester Institute of Biotechnology, and ⁶Department of Chemistry, University of Manchester, Manchester, UK

Reviewed by members of the JBC Editorial Board. Edited by Chris Whitfield

Many bacterial species are known to recover peptidoglycan (PG) fragments released from remodeling of their cell walls during growth and cell division. These PG fragments not only provide an essential energy resource, especially in nutrient restricted environments, but also play a critical role in influencing infection. Yet whether mycobacteria have the capacity to recycle their PG, or not, has still not been resolved. In this study, we show that NagA, an N-acetylglucosamine-6phosphate (GlcNAc-6-P) deacetylase, is essential for coordinating the remodeling and recycling of an amino sugar component released from the mycobacterial cell wall. We show that NagA is exclusively responsible for GlcNAc-6-P deacetylation and is pivotal for the de novo synthesis of core cell wall building blocks. Indeed, a nagA deletion mutant exhibited an altered composition of the cell envelope, smaller overall cell size, defective biofilm formation, and enhanced susceptibility to cell wall targeting agents. Moreover, uptake analysis and profiling of the amino sugar pool revealed that NagA inactivation blocks *N*-acetylglucosamine (GlcNAc) import and has a pronounced effect on the fate and levels of the intracellular amino sugar pool. Loss of NagA led to the upregulation and downregulation of proteins involved in cell wall biosynthesis, thereby altering cell wall homeostasis. Overall, our data highlight the importance of an overlooked yet conserved component in an important PG salvage pathway in mycobacteria, in which NagA provides a unique GlcNAc sensing mechanism, thus acting as a checkpoint for regulating the recovery and reuse of PG fragments.

Mycobacterium tuberculosis (Mtb), the causative agent of tuberculosis (TB) is, arguably, one of the world's most successful pathogens globally, responsible for over ~1 billion deaths over the last 2000 years (1). The World Health

Organization estimates that in 2023 there were \sim 10.8 million new active TB cases and 1.3 million deaths resulting from TB infection, placing Mtb as one of the leading causes of death from a single infectious agent worldwide (https://www.who. int/tb/publications/global_report/en/). Although there are effective treatment regimens against drug-susceptible TB, poor compliance and the lack of new therapeutic options have led to the emergence and escalation of not only drugresistant, but also untreatable strains of Mtb, which is jeopardizing efforts to control the TB epidemic (2). Clearly, there is an urgent need to identify alternative pathways that can be targeted with novel treatment strategies to combat this major global health challenge.

One of the distinguishing features of the Mtb pathogen is a highly unique cell envelope, which is integral to its virulence and survival (3-5). Given its essentiality, cell wall synthetic pathways have been exploited as targets of many current firstand second-line TB therapeutics, as well as those under development in the drug development pipeline. Yet despite this vulnerability, not all the pathways involved in cell wall synthesis have been explored or targeted. The mycobacterial cell wall is a complex macromolecular structure comprising of an interconnected peptidoglycan, arabinogalactan and long chain mycolic acid (mAGP) core, interspersed with additional "free" lipids and glycolipids that form an outer "myco-membrane" and an outer capsule composed predominantly of an α -glucan polysaccharide (3–5). The inner peptidoglycan (PG) mesh acts as an attachment scaffold for arabinogalactan (AG) and has a substantial role in the structural integrity and tensile strength of the cell and protection against osmotic pressure. In mycobacteria, PG consists of glycan strands of an alternating $\beta(1 \rightarrow 4)$ linked N-acetylglucosamine (GlcNAc) to either an N-acetylmuramic acid (MurNAc) or an N-glycolyl derivative (MurNGly), distinguishing it from other bacterial species, with adjacent chains cross-linked through short peptide chains (6, 7). Further modifications are *via* a unique α -1-rhamnopyranose- $(1 \rightarrow 3)$ - α -D-GlcNAc- $(1 \rightarrow P)$ linker unit,

[‡] These authors contributed equally and listed in alphabetical order.

^{*} For correspondence: Elizabeth Fullam, elizabeth.fullam@manchester.ac.

which attaches approximately 10 to 12% of the muramic acid residues of PG to AG (8).

In mycobacteria the biosynthesis of PG and the unit linking PG to AG both require the UDP-GlcNAc building block, the de novo synthesis of which relies on the supply of the glucosamine-6-phosphate (GlcN-6-P) precursor, which sits at the crossroads of the glycolysis and cell wall biosynthetic pathways (Fig. 1) (9). GlcN-6-P is generated either from the glycolysis pathway, where GlmS catalyzes the isomerization of fructose-6-phosphate to GlcN-6-P (10, 11), or alternatively GlcN-6-P can be derived from the deacetylation of GlcNAc-6-P by NagA (12, 13). Because there are no obvious GlcN-6-P acetyltransferases in mycobacteria (14), the most likely origin of cytosolic GlcNAc-6-P is through the recycling, import and phosphorylation of GlcNAc released from remodeled PG. GlcN-6-P is subsequently converted to UDP-GlcNAc in three steps via the formation of glucosamine-1-phosphate (GlcN-1-P) and the N-acetyl-glucosamine-1-phosphate (GlcNAc-1-P) intermediate (Fig. 1) by the sequential action of GlmM and GlmU (15–17). The UDP-GlcNAc building block is then utilized to form the cell wall.

In various bacterial species, the NagA pathway has been shown to have an important role in a plethora of processes that range from regulating GlcNAc assimilation and metabolism; triggering cell signaling pathways, perturbing the intracellular amino sugar pool; maintaining cell wall

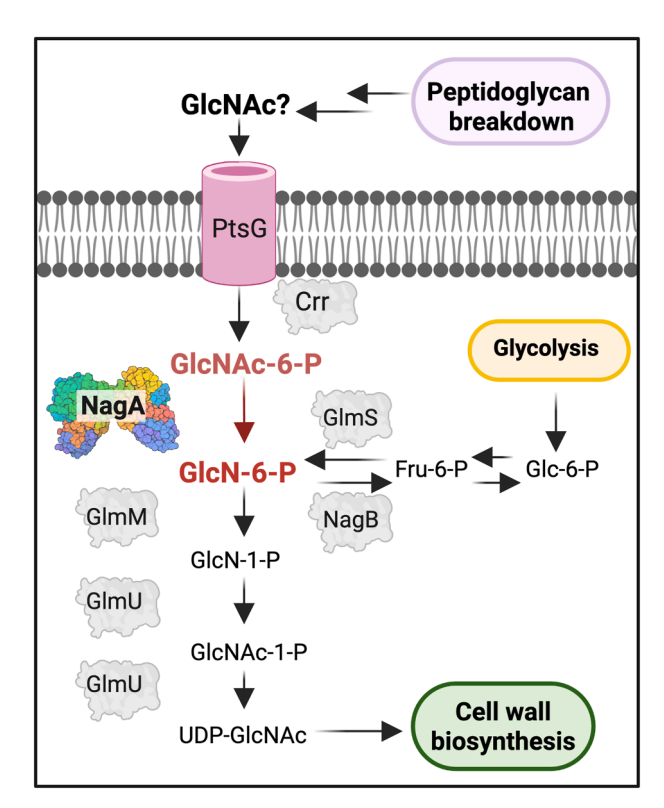


Figure 1. Overview of the GlcNAc recycling pathway in *Mycobacterium. smegmatis.* In *M. smegmatis* GlcNAc is likely imported by PtsG and phosphorylated by Crr to form GlcNAc-6-P and further deacetylated by NagA to glucosamine 6-phosphate (GlcN-6-P). The pathway then diverges, and GlcN-6-P is either shunted into cell wall biosynthesis or converted to fructose 6-phosphate (Fru-6-P) by the action of NagB to enter the glycolysis pathway. Created with BioRender.

biosynthesis and homeostasis, coordinating PG recycling and, in Streptomyces, controlling antibiotic production (18-26). The exogenous supply of GlcNAc is likely derived predominantly from core bacterial cell wall components, and pathways to recover GlcNAc and other PG fragments to ensure scarce resources are not otherwise lost are well established in many bacterial species. However, the mechanisms that mycobacteria deploy to recycle their cell walls are less clear, despite mycobacterial PG metabolites enabling key aspects of Mtb biology, such as resuscitation, virulence, cell division, and cell wall synthesis (27-30). Although the complete repertoire of mycobacteria cell wall recycling enzymes has not yet been identified, an exception is NagA. We have previously shown that the mycobacterial NagA enzyme is responsible, and selective, for the deacetylation of GlcNAc-6-P (12). But very little is known about the role of NagA in mycobacterial cells; however, proteomic profiling identified NagA is present in lung tissues from guinea pigs infected with Mtb, pointing toward a potential role in Mtb during infection (31). In addition, nagA is highly conserved across mycobacterial species, including Mycobacterium leprae, an obligate pathogen that has undergone extensive gene decay resulting in a core set of genes considered essential to facilitate intracellular survival in humans (Fig. S1) (32), providing evidence that the NagA pathway is also an important metabolic process for mycobacteria.

In this study, we sought to investigate the role of the previously overlooked NagA enzyme in *Mycobacterium smegmatis*. We demonstrate that NagA is indeed exclusively responsible for the GlcNAc-6-P deacetylase activity in mycobacterial cells and provide evidence linking its function to GlcNAc uptake and regulation of intracellular levels of the amino sugar pool. Loss of NagA activity resulted in defective PG biosynthesis leading to increased susceptibility to PG targeting agents, smaller cells, and impaired biofilm formation, underscoring its role in maintaining cell wall homeostasis. Overall, our data indicate that NagA is a key player in recycling remodeled PG fragments in mycobacteria, contributing to the control and use of scarce nutrient resources during infection.

Results

NagA is required for the deacetylation of GlcNAc-6-P

To assess the importance of GlcNAc-6-P deacetylase activity in mycobacteria, we constructed an in-frame deletion mutant of *nagA* in *M. smegmatis*, which was confirmed by whole genome sequencing (Fig. S2) and expression of the adjacent genes from extracted RNA (Fig. S2). To validate NagA function in *M. smegmatis*, we monitored GlcNAc-6-P deacetylase activity in cell lysates, which fell from 32.9 nmol/min/mg of protein in the WT strain to undetectable levels in the mutant. This activity is consistent with our prior biochemical data (12), indicating that under the conditions tested NagA is the only enzyme responsible for the deacetylation of GlcNAc-6-P in mycobacterial cells and establishes that this activity is not functionally compensated by

other pathways, despite the high level of genetic redundancy in M. smegmatis.

NagA is essential for utilizing GlcNAc as a sole carbon source

To determine the impact of *nagA* deletion on the ability of M. smegmatis to utilize various carbon sources, strains were starved and growth assessed after 7 days in minimal media supplemented with glycerol (Gly), glucose (Glc), glucose 6-phosphate (Glc-6-P), fructose 6-phosphate (Fru-6-P), glucosamine (GlcN), GlcN-6-P, GlcNAc, and GlcNAc-6-P. Wild type (WT) M. smegmatis preferentially utilized Glc > GlcN-6-P > Gly > GlcN > GlcNAc > Glc-6-P as a sole carbon source but did not grow on GlcNAc-6-P or Fru-6-P supplemented media (Fig. 2A). The pattern of carbon source utilization for $\Delta nagA$ mirrored the parental strain except for GlcNAc, where the WT strain grew but $\Delta nagA$ did not. To analyze if the growth defect occurred during all growth phases, we monitored the absorbance during the lag phase and transition to exponential growth and found $\Delta nagA$ still failed to grow (Fig. 2B). Next, to examine whether NagA inactivation causes bacteriostasis or lethality in M. smegmatis, we monitored the ability to form colony forming units (CFUs). No significant differences in the viability of both strains were observed following nutrient starvation or growth

in minimal media over the experimental time course (Fig. S3). As expected, the CFUs increased for the WT strain supplemented with GlcNAc but not for $\Delta nagA$, which remained viable but static (Fig. S3), suggesting that under these low nutrient conditions an impaired ability to use GlcNAc by the $\Delta nagA$ mutant is responsible for the observed phenotype. When supplied with glucose, its preferred carbon source, and GlcNAc, a dual carbon condition that promotes the induction of nagA and incorporation of exogenous GlcNAc into PG (33), we found enhanced growth of the WT strain (Fig. 2C). In contrast the nagA mutant consistently reached lower biomass levels under these conditions, with a growth phenotype that closely resembles that of cells grown with glucose alone (Fig. 2C). Taken together, this strongly suggests that NagA has a pivotal role in GlcNAc utilization and controlling mycobacterial growth in response to exogenous GlcNAc availability.

NagA controls GlcNAc uptake and the incorporation of exogenous GlcNAc into the cell wall

Because our growth phenotypes indicate NagA controls how M. smegmatis accesses GlcNAc, we wanted to determine whether inactivation of GlcNAc-6-P deacetylase activity influences the entry of this amino sugar into the cell. To test

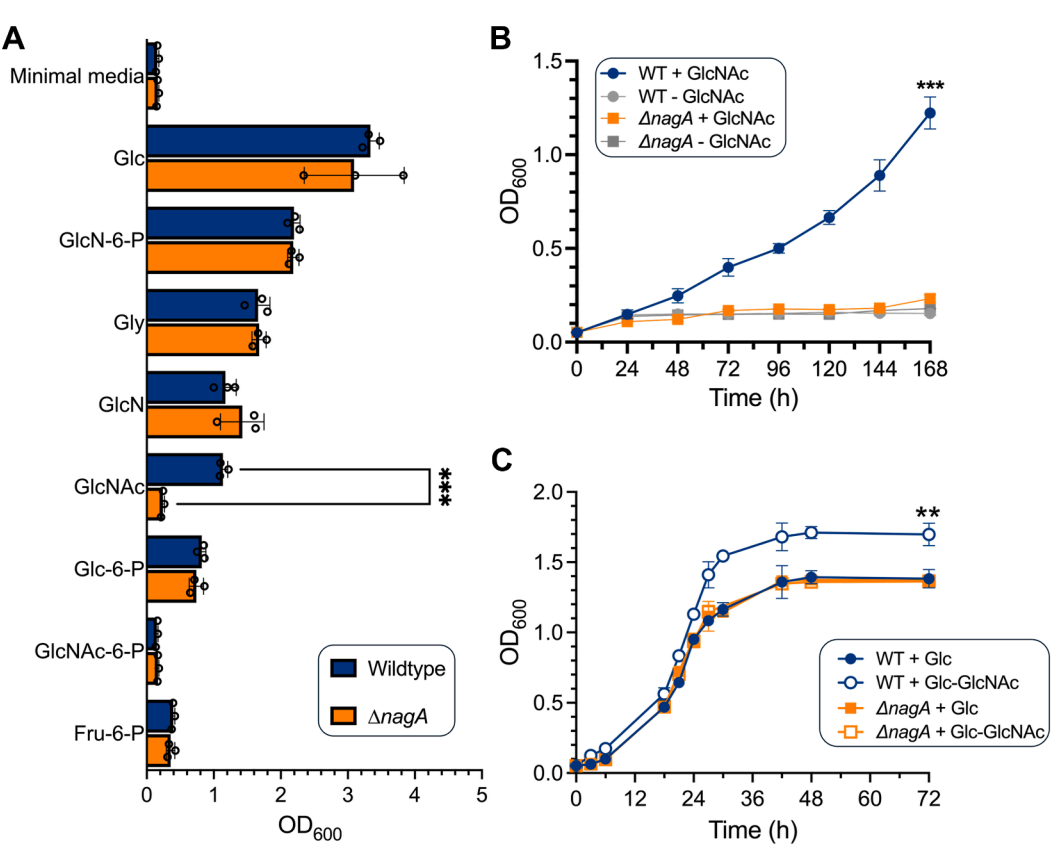


Figure 2. GlcNAc availability and use by NagA influences mycobacterial growth. A, growth at 7 days of WT (blue) and Δ nagA (orange) in minimal media supplemented with 20 mM glucose (Glc), glucosamine 6-phosphate (GlcN-6-P), glycerol (Gly), glucosamine (GlcN), N-acetyl glucosamine (GlcNAc), glucose 6-phosphate (Glc-6-P), glucosamine 6-phosphate (GlcN-6-P), N-acetyl glucosamine 6-phosphate (GlcNAc-6-P), fructose 6-phosphate (Fru-6-P), B, growth curves of WT (blue) and \(\Delta nagA \) (orange) in minimal media in the presence or absence of 20 mM GlcNAc. C, growth curves of WT (blue) and AnagA (orange) in minimal media supplemented with either 5 mM glucose or 5 mM glucose and 1 mM GlcNAc. Error bars represent standard deviation from three biological replicates. Statistical significance was determined using unpaired t-tests * = p < 0.05, ** = p < 0.01 *** = p < 0.001.



this, we performed uptake assays with $^{14}\text{C-GlcNAc}$ in mid-log phase WT and $\Delta nagA$ cells. Radiolabeled GlcNAc was rapidly taken up in WT with a rate of 7.3 \pm 0.3 pmol/min/ 10^9 CFU, whereas much lower levels of this amino sugar accumulated in the nagA mutant, and its uptake rate was much slower (1.4 \pm 0.1 pmol/min/ 10^9 CFU) (Fig. 3A). Cells grown in the presence of both Glc and GlcNAc displayed an \sim 1.3-fold increase in uptake rate (9.7 \pm 0.4 pmol/min/ 10^9 CFU) in WT, whereas a \sim 2.3-fold (0.6 \pm 0.2 pmol/min/ 10^9 CFU) reduction was observed in $\Delta nagA$ (Fig. 3A).

As GlcNAc is ultimately incorporated into the mycobacterial cell wall, predominantly as PG but also in the GlcNAc linker unit of AG, we then asked if impaired GlcNAc-6-P deacetylase activity disrupts the intracellular processing of this amino sugar building block. Following exposure to ¹⁴C-GlcNAc, we mapped the fate of the radiolabel by analyzing the incorporation of radioactivity into isolated cytosolic, PG and AG components from WT and the nagA mutant (Fig. 3B). As a proportion of the total cellular uptake, ¹⁴C-GlcNAc, or ¹⁴C-GlcNAc metabolite/s, accumulated at much higher levels in the cytosol of the *nagA* deletion mutant. Also, the $\Delta nagA$ strain showed a pronounced reduction in 14C-labeled PG. Surprisingly, AG extracted from $\Delta nagA$ showed a higher ratio of ¹⁴C-labeled AG to PG, indicating that loss of NagA activity leads to the UDP-GlcNAc cell wall precursor, common to both AG and PG pathways, being preferentially directed to form the linker unit attaching arabinan to PG. Collectively, this provides evidence that NagA acts a gatekeeper that regulates the recycling of PG derived amino sugars and maintains cell wall homeostasis.

Deletion of nagA increases susceptibility to cell wall targeting agents

We reasoned that reduced incorporation of ¹⁴C-GlcNAc into the cell-envelope may lead to defects or alterations that modify its sensitivity to antibiotics and cell wall targeting agents. To probe this further, we assessed susceptibility of the *nagA* deletion strain against a panel of antibiotics and cell wall targeting agents by the resazurin microtitre assay (Table S1). We found that deletion of *nagA* resulted in increased

susceptibility to the PG targeting agents vancomycin, cycloserine, and lysozyme; β-lactams in the presence of the β-lactamase inhibitor clavulanic acid; and the cell wall synthesis inhibitors isoniazid and ethambutol (Table S1 and S2). Spot assays confirmed the observed two-fold reductions in minimum inhibitory concentrations (MICs) with reduced recovery for the $\Delta nagA$ strain for each antibiotic, except ethambutol (Table S3). The discrepancy for ethambutol may be due to differences in its availability in agar versus liquid broth. No changes in the MICs for other antibiotic classes between the two strains were observed. To assess the integrity of the cell wall we tested the susceptibility of $\Delta nagA$ to lysis after incubation with lysozyme and found a significant reduction in survival of the nagA deletion mutant compared to the WT strain (Fig. S4A). This increased susceptibility is not due to a change in cell wall permeability as determined by ethidium bromide uptake (Fig. S4B). Additional lipid profiling revealed no qualitative differences of the $\Delta nagA$ mutant grown in vitro (Fig. S5), and comparable levels of Congo red staining for both strains (Fig. S4C) suggesting that the lipid layers of the cell wall are not altered upon nagA deletion. Collectively, these results demonstrate that deletion of nagA impairs the mycobacterial cell wall integrity, predominantly by altering PG formation.

PG composition of mid-log phase M. smegmatis is altered by the deletion of NagA

Given the increased susceptibility of the *nagA* mutant to PG-targeting agents, we hypothesized that NagA activity influences the structure and composition of mycobacterial PG. To test this, WT and $\Delta nagA$ cells were cultured to mid-log and stationary phases with or without the addition of GlcNAc, and their extracted PG was analyzed using liquid chromatographytandem mass spectrometry (LC-MS/MS). Across all samples, 29 PG monomers and 20 PG dimers were identified (Table 1, Fig. S6). For both strains the predominant muropeptide species were monomers (\sim 74–87%) (Table 1). In exponential growth the *nagA* mutant displayed an altered PG profile compared to WT. When grown in the presence of GlcNAc, the $\Delta nagA$ strain exhibited a higher dimer-to-monomer ratio (\sim 1:3) compared to

AnagA

AG

PG

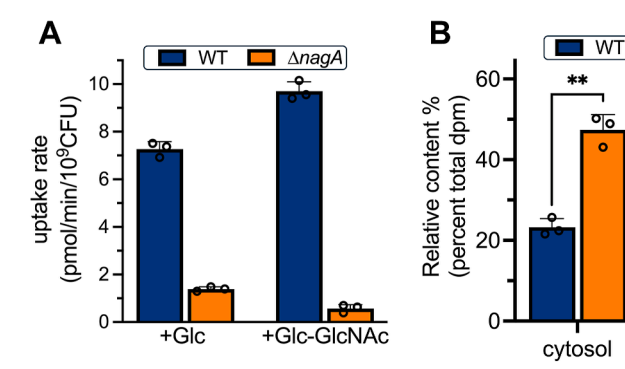


Figure 3. Deletion of nagA prevents 14 C-GlcNAc uptake and alters incorporation of exogenous 14 C-GlcNAc into cell walls. A, GlcNAc uptake rates in wild type and Δ nagA strains grown in minimal media supplemented with either 5 mM glucose or 5 mM glucose and 1 mM GlcNAc; B, incorporation of 14 C-GlcNAc into the cytosol, arabinogalactan (AG), and peptidoglycan (PG) of Mycobacterium smegmatis. WT and Δ nagA grown in minimal media with 5 mM glucose and 1 mM GlcNAc. Error bars represent standard deviation from three biological replicates. Statistical significance was determined using unpaired t-tests *=p < 0.05, **=p < 0.01 *** = p < 0.001.

Table 1 Peptidoglycan composition of WT and $\Delta nagA$ strains

| Muropeptide | 18 h + GlcNAc | | 18 h - GlcNAc | | 48 h + GlcNAc | | 48 h - GlcNAc | |
|---------------------|------------------|---------------|------------------|---------------|------------------|---------------|------------------|---------------|
| | WT | $\Delta nagA$ |
| % monomers | 85.8 | 74.4 | 84.3 | 83.2 | 85.3 | 86.2 | 87.3 | 82.7 |
| % dimers | 14.2 | 25.6 | 15.7 | 16.8 | 14.7 | 13.8 | 12.7 | 17.3 |
| Dimer:monomer ratio | 1:6.0 | 1: 2.9 | 1:5.4 | 1:5.0 | 1:5.8 | 1:6.2 | 1:6.9 | 1:4.8 |
| GlcNAc-MurGlyc (%) | 93.3 | 98.6 | 45.7 | 64.2 | 99.4 | 99.6 | 98.6 | 98.6 |
| GlcNAc-MurNAc (%) | 6.3 | 0.5 | 32.6 | 22.9 | 0.4 | 0.2 | 0.7 | 0.5 |
| GlcNAc-Mur (%) | 0.4 | 1.0 | 21.8 | 12.9 | 0.2 | 0.1 | 0.8 | 0.7 |

The full list of monomers and dimers identified by LC-MS/MS are shown in Supplementary file S3.

GlcNAc, N-acetylglucosamine; MurNAc, N-acetylmuramic acid; MurGlyc, N-glycolylated muramic acid; Mur, muramic acid.

the WT strain (\sim 1:6) indicating a higher extent of crosslinking in the mutant. In the absence of GlcNAc, the $\Delta nagA$ mutant peptidoglycan showed a higher abundance of glycolylated muramic acid (~64% versus 46% for WT) along with a reduced abundance of acetylated muramic acid (23% versus 33% for WT) and deacetylated MurNAc (\sim 13% *versus* 22% of MurN for WT). These findings suggest that disruption of NagA alters the PG composition and polymerization, which may impact the integrity and physical properties of the cell envelope.

Deletion of nagA results in shorter cells and altered cell wall thickness

Since the PG composition of the $\Delta nagA$ strain differs from that of the WT and given the critical role of PG composition and architecture in maintaining bacterial cell shape (34) we investigated NagA's role in defining mycobacterial cell morphology. WT and $\Delta nagA$ strains were cultured in Sauton's minimal media supplemented with either glucose or glucose and GlcNAc and their morphology assessed during mid-log and stationary growth phases. Imaging cell flow cytometry revealed that $\Delta nagA$ cells were significantly shorter than WT cells in mid-log-phase, regardless of GlcNAc presence. (Fig. 4). In contrast, no differences in cell size were observed between the strains in stationary phase, when no cell division occurs (Fig. 4). To probe this result further, transmission electron microscopy (TEM) was used to examine the ultrastructure of the cell wall. As expected, WT cells exhibited normal morphology characterized by an inner electron dense layer (EDL) which corresponds to PG, an electron translucent layer representing the mycolyl-arabinogalactan and an outer EDL consisting of external lipids (35–37) (Figs. 4B and S7–S10). In contrast, as shown in Figure 4C, the $\Delta nagA$ the mutant strain exhibited notable morphological changes with a much thicker inner EDL and a reduced electron translucent layer, while the outer EDL remained similar to WT cells, consistent with our lipid analyses (Fig. S5). This indicates that nagA cells have a thicker PG layer and smaller AG region than WT cells. Together, these data point toward NagA's involvement in controlling cell shape and morphology during cell-division.

Deletion of nagA leads to the altered abundance of PG recycling and synthesis pathway metabolites

As we observed a pronounced reduction in GlcNAc uptake, alongside the substantial accumulation of 14C in the cytosol and altered cell wall in $\Delta nagA$, we hypothesized that the intracellular amino sugar pool of the nagA mutant might be perturbed. To test this hypothesis, we quantified the amino sugars immediately upstream and downstream of NagA, in WT and mutant cytosolic extracts by ion chromatography with pulsed amperometric detection (Fig. 5). Inactivation of NagA led to an extensive build-up of GlcNAc-6-P (Fig. 5A), whereas the intracellular GlcN-6-P pool was completely depleted (Fig. 5B) even though this metabolite can also be produced by the glycolytic pathway. Although GlcNAc is thought to be internalized via a phosphoenolpyruvatedependent sugar phosphotransferase system (PTS) in M. smegmatis, we unexpectedly observed a substantial accumulation of GlcNAc, rather than GlcNAc-6-P, in $\Delta nagA$ cells grown in the presence of exogenously supplied GlcNAc (Fig. 5C) suggesting additional routes for GlcNAc assimilation. Collectively, these findings establish that inactivation of NagA perturbs the intracellular reservoir and the generation of key amino sugar precursors thus regulating amino sugar flux.

NagA deacetylase activity is required for biofilm formation

Because impaired PG biosynthesis is known to result in defective biofilms (38, 39), we speculated that blocking the NagA PG recycling pathway might also be key for biofilm formation. We assessed the formation of WT and $\Delta nagA$ pellicular biofilms formed at the air-liquid interface over 7 days. As shown in Figure 6, while biofilms of the nagA mutant strain could be observed, they exhibit a much smoother, more fragile morphology in contrast to the characteristic robust, wrinkled biofilms of WT. Next, we wanted to establish if elevated exogenous GlcNAc levels impacted on biofilm formation in both strains. We found that the WT strain switched biofilm phenotype, which now closely resembles the smooth morphology seen in the *nagA* mutant, while the biofilm phenotype of $\Delta nagA$ is further accentuated (Fig. 6A). Crystal violet quantification showed a significant reduction in the biofilm biomass of Δ nagA compared to WT under both conditions (Fig. 6B). In contrast, the total biomass amount for WT or $\Delta nagA$ was similar regardless of the presence or absence of GlcNAc (Fig. 6B). To determine whether the altered biofilm biomass is linked to viability, we assessed CFU counts and found no differences between the WT and nagA



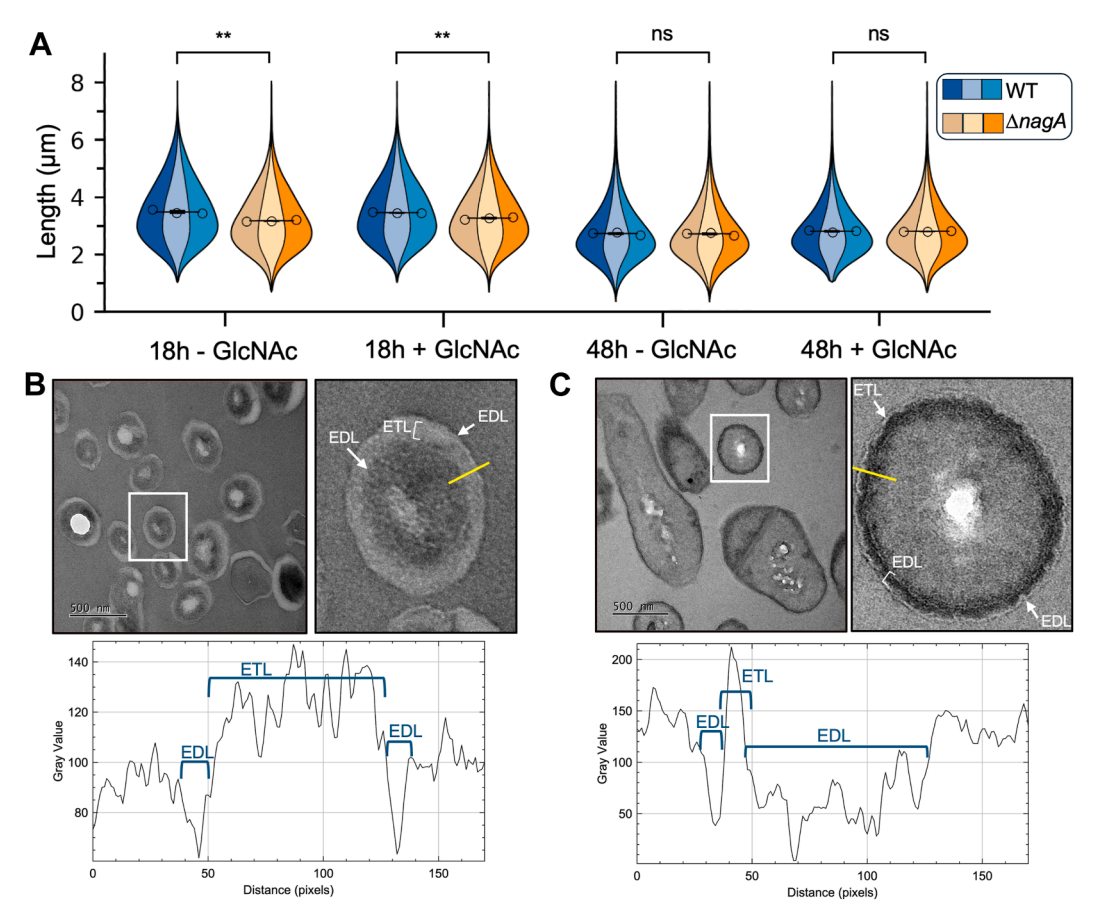


Figure 4. NagA influences mycobacterial cell morphology. WT and $\Delta nagA$ strains were grown in Sauton's media supplemented with either glucose (5 mM) or glucose (5 mM) and GlcNAc (1 mM) and analyzed by imaging flow cytometry and TEM at 18 h and 48 h. *A*, cell length; error bars represent standard deviation from three biological replicates. Statistical significance was determined using unpaired *t*-tests * = p < 0.05, ** = p < 0.01 *** = p < 0.001. Plots were made with the superviolin package in Python3.x Miniconda. *B*, TEM images of WT (18 h; Sauton's minimal media supplemented with 5 mM glucose (5 mM) and GlcNAc (1 mM)). *C*, TEM images of $\Delta nagA$ (18 h; Sauton's minimal media supplemented with 5 mM glucose (5 mM), and GlcNAc (1 mM) GlcNAc. The white square indicates the cell zoomed in on. Gray scale intensity plots measured across the *yellow dashed line*. Additional TEM images for WT and $\Delta nagA$ strains at 18 h and 48 h are shown in Figs. S7-510. Fig. 4*B* is included in Fig. S8A. Fig. 4C is included in Fig. S8B. EDL, electron dense layer; ETL, electron translucent layer; TEM, transmission electron microscopy.

mutant, indicating that impaired biofilm formation is not a consequence of changes in bacterial growth rate or viability (Fig. 6C). These findings demonstrate the crucial importance of NagA activity for effective biofilm formation.

Global proteomic analysis revealed NagA influences PG, AG, and capsular glucan pathways

Next, to examine the effect of nagA disruption on wider biosynthetic pathways, we performed whole cell proteomics of mid-exponential WT and $\Delta nagA$. Differential expression

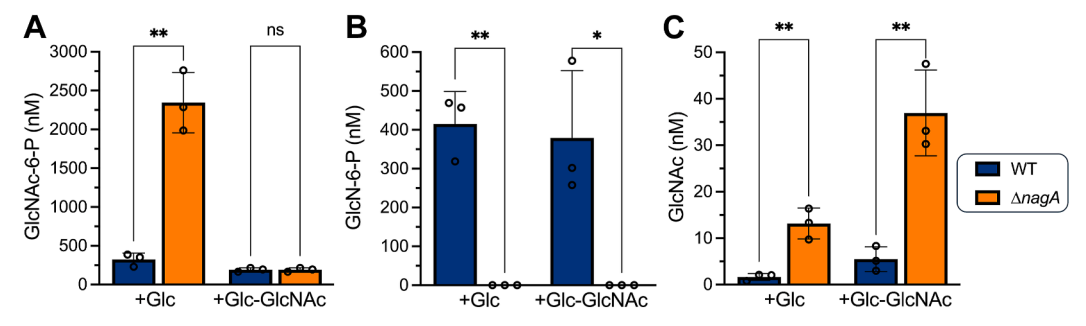


Figure 5. NagA catalysis of GlcNAc-6-P is required to maintain the intracellular amino sugar pool. High-performance anion-exchange chromatograph with pulsed amperometric detection (HPAEC-PAD) analysis of WT and $\Delta nagA$ cytosolic extracts of strains grown in minimal media supplemented with either 5 mM glucose or, 5 mM glucose and 1 mM GlcNAc. A, cytosolic GlcNAc-6-P concentration B, cytosolic GlcN-6-P concentration, C, cytosolic GlcNAc concentration. Error bars represent standard deviation from three biological replicates. Statistical significance was determined using unpaired t-tests * = p < 0.05, ** = p < 0.01 *** = p < 0.001.

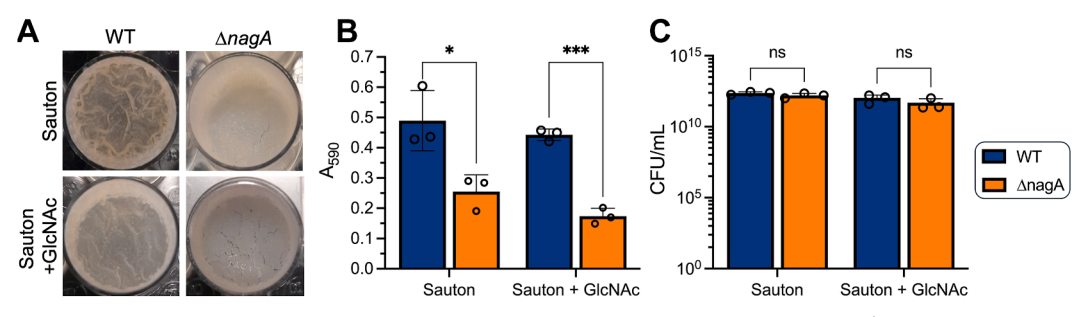


Figure 6. The nagA deletion mutant exhibits a defect in biofilm formation. A, images of 7-day old WT and $\Delta nagA$ biofilms grown in detergent-free Sauton media in the presence or absence of 20 mM GlcNAc, B, crystal violet biofilm quantification, C, colony forming unit (CFU) enumeration of strains after 7 days of biofilm formation. Error bars represent SD from three biological replicates. Statistical significance was determined by unpaired t tests * = p< 0.05, ** = p < 0.01, and *** = p < 0.001.

analysis revealed that 76 proteins are found in higher abundance and 38 proteins in lower abundance in the nagA mutant based on a log2 fold change (FC) $> \pm 1$ and adjusted p value ≤ 0.05) (Fig. 7, Supplementary File S4). Most notably, the nagA mutant showed pronounced changes in the abundance of specific enzymes in the PG and AG biosynthetic pathways. Specifically, we found over four-fold higher levels of WbbL1 (MSMEG_1826) in the nagA deletion mutant. WbbL1 is responsible for the formation of the AG-PG linker (40). This finding is consistent with our radiolabeling studies that showed $\Delta nagA$ preferentially funnels 14C-GlcNAc into AG rather than PG. In contrast, we observed a ~4-fold reduction in the levels of the D-alanyl-D-alanine carboxypeptidase DacB2 (MSMEG_2433), involved in removing the terminal Dalanine residue from the pentapeptide sidechains (41), and a \sim 2-fold reduction in levels of the probable penicillin binding protein transpeptidase Pbp3 (MSMEG_4233, Rv2163c). Examination of the proteins encoded in the nagA operon revealed unaltered levels of Crr (MSMEG 2117) and a significant 1.8-fold increase in abundance for (MSMEG_2119). NagB funnels GlcN-6-P into the glycolysis pathway (Fig. 1), suggesting a mechanism to regulate the intersecting cell wall biosynthesis and glycolysis pathways in the absence of NagA. The $\Delta nagA$ strain also showed pronounced alterations of proteins levels involved in the biosynthesis of other mycobacterial envelope cell

constituents. The abundance of GlgE, (MSMEG_4916), involved in the glucan capsule synthesis (42) increased ~10fold, whereas Ag85C (MSMEG 6583), responsible for trehalose mycolate synthesis (43) showed a significant decrease of \sim 7-fold. Combined, our findings further point toward a global role for NagA in maintaining cell wall homeostasis.

Discussion

Many bacteria remodel and recycle as much as 30 to 50% of the PG cell wall polymer during one generation of growth (44). This process prevents the loss of a substantial carbon and nitrogen resource that would otherwise be lost, for use either as an energy source or for the synthesis of more PG. However, PG remodeling in mycobacteria remains unresolved. This is despite mycobacteria encoding the glycosidase, amidase, endopeptidase, and carboxypeptidase machinery to breakdown its PG, producing an array of fragments that have pivotal roles throughout the pathogen's lifecycle (45). Specifically, the mycobacterial recycling route/s for the exogenous PG breakdown products are not well defined and whether these PG metabolites are reused, or not, is not clear. Although import systems to salvage GlcNAc in other bacterial systems are known, the fate of GlcNAc in mycobacteria is less clear and appears to be influenced by the conditions encountered (46, 47). One potential route for mycobacteria to recover its PG is via the highly conserved Mtb UspABC ATP-

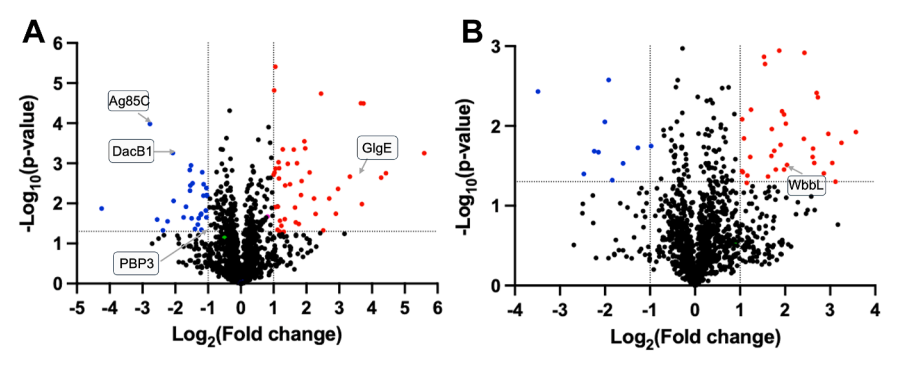


Figure 7. Comparative proteomic analysis of Mycobacterium smegmatis WT and the nagA deletion mutant. Volcano plots illustrating the differential protein abundance of (A) soluble and (B) membrane proteins between the WT and nagA deletion mutant strains. Blue corresponds to proteins with significant (p = < 0.05) $< -1 \log_2$ fold change abundance. Red corresponds to proteins with significant (p = < 0.05) $>1 \log_2$ fold change abundance. Proteins involved in cell wall synthesis pathways are highlighted. The full proteomics dataset is listed in Supplementary file S4.



binding cassette (ABC)-transporter, which has been implicated in the recognition of amino sugars (48). Yet little is known regarding the identity of other mycobacterial PG recycling systems as there are no obvious orthologues encoded within the mycobacterial genome. Furthermore, computational analyses suggest that PG salvage pathways differ between mycobacterial species, making it more difficult to infer function. For instance, the organization of the NagA PG recovery pathway varies among different species (Fig. S1). In M. smegmatis a putative amino PTS, PtsG-Crr, system is present within the genetic locus encoding nagA, pointing toward an additional route for GlcNAc reuse whereas no obvious PTS exist in Mtb (14, 49). In contrast, ptsG and crr are absent in Mtb, and instead sugI is located adjacent to nagA. SugI is a putative major facilitator superfamily transporter, so may have a role in amino sugar assimilation in Mtb, and further experiments are underway to investigate this further. Whether additional import systems for GlcNAc and/ or other PG fragments exist remains to be elucidated.

To investigate PG recycling in mycobacteria we characterized the role of the highly conserved NagA enzyme as part of an unexplored, potential pathway for PG recovery (Fig. 1). In this study, a combination of genetic and biochemical studies revealed that NagA does indeed have a key role in controlling the fate and recovery of exogenous GlcNAc in M. smegmatis and is required for normal cell wall synthesis and biofilm formation. Even though NagA has a key role that acts as a gatekeeper between the cell wall biosynthesis and glycolysis pathways, it is solely responsible for catalyzing the deacetylation of GlcNAc-6-P to the essential GlcN-6-P amino sugar in the cell and no other enzyme can substitute for this function. Furthermore, our combined growth, uptake, and metabolite analyses all point toward an additional broader role of NagA (Figs. 2, 3 and 5). The inability of the nagA mutant to utilize GlcNAc as a sole carbon source (Fig. 2) was surprising given that NagA is not a transporter, which implies that NagA controls GlcNAc import via alternative mechanisms. A possible explanation for this emerged from our observation that the nagA mutant accumulates millimolar levels of GlcNAc-6-P in the absence of NagA (Fig. 5). As GlcNAc-6-P accumulation is toxic in Escherichia coli and Streptomyces (24, 50), it could therefore be envisaged that NagA tightly regulates the uptake and metabolism of GlcNAc as a self-protection mechanism to prevent the toxic build-up of GlcNAc-6-P in M. smegmatis cells. This process may potentially be driven by a self-amplifying feedback loop that signals to decrease GlcNAc uptake depending on the external and internal levels of GlcNAc and associated pathway metabolites. Our uptake experiments corroborate this observation as the rate and amount of 14C-GlcNAc uptake in the nagA mutant was significantly reduced (Fig. 3), whilst the slightly increased uptake of 14C-GlcNAc by the WT strain in the presence of GlcNAc may reflect induction of nagA under these conditions, which has been reported previously (33, 51). A similar phenotype has been observed for Streptomyces species where GlcNAc levels act as a master switch that signals for growth development and antibiotic production depending on the nutritional status of the environment (23, 52). This implies that both the environmental resources and the metabolic status of the intracellular amino sugar pool serve as a cue that regulates GlcNAc signaling and reuse in M. smegmatis. As GlcN-6-P can still be generated from the glycolysis pathway by the action of GlmS, it is intriguing that the intracellular levels of GlcN-6-P are not maintained (Fig. 5). Instead, the GlcN-6-P pool is completely depleted in the nagA deletion mutant (Fig. 5), below the limits of highperformance anion-exchange chromatography detection, highlighting that both the NagA and glycolysis pathways make important contributions in maintaining the intracellular reserves of GlcN-6-P. Because GlcN-6-P is an essential metabolite it is conceivable that mycobacteria cannot afford to retain surplus of GlcN-6-P when the NagA pathway is inactive. Instead, it is likely that once synthesized, GlcN-6-P is rapidly channeled into the cell wall, although it appears that GlcN-6-P levels are not sufficient to maintain proper cell wall homeostasis. GlcN-6-P levels are further reduced in $\Delta nagA$ by reprogramming of the glycolysis pathway (Fig. 7). GlmS is downregulated (FC: -1.4, p-value: 0.07), whereas the reverse reaction catalyzed by NagB is upregulated (FC: 1.8, p-value: 0.02) (Fig. 7) thereby reducing the flux of GlcN-6-P into cell wall biosynthesis. Hence, the crosstalk between cell wall biosynthesis and glycolysis, controlled by NagA, leads to diminished GlcN-6-P availability, which may cause an imbalance in GlcN-6-P consumption in these interlinked and competing pathways. An important consequence of impeded NagA activity is the altered fate of the GlcNAc metabolite. In the nagA mutant the 14C-GlcNAc that is imported accumulates at very high levels in the cytosol rather than in the cell wall (Fig. 3). The pronounced difference in the 14C-label incorporation pattern in $\Delta nagA$ was not as expected, with comparable ¹⁴C-levels within the PG and the AG linker unit (Fig. 3), implying significant defects in cell wall biosynthesis. Given that AG anchoring to PG is essential for mycobacterial survival (53) our findings imply that when the NagA PG recycling pathway is disrupted, mycobacteria prioritize synthesis of the entire AG linker unit over PG to prevent disruption of this extremely vulnerable pathway. This correlates with $\Delta nagA$'s increased sensitivity to antimicrobials (Table S1), particularly PG targeting agents. Indeed, our PG fragment analysis and TEM studies further support this, revealing substantial structural and compositional changes in the mutant's PG and a reduction in cell size (Fig. 4). We suggest that the compromised cell wall integrity in the nagA mutant triggers a compensatory mechanism that reinforces the PG layer, resulting in its thickening and increased peptide cross-linking to maintain cell fitness. In addition, beyond the PG layer, the *nagA* mutant exhibits a much thinner mycolylarabinogalactan layer (Fig. 4). The reduction is likely due to alterations in the PG structure, which may limit the availability of AG attachment sites, leading to decreased incorporation of AG in the cell wall. Together with the nagA mutant's increased sensitivity to ethambutol (Table S1), a front-line TB drug that targets AG biosynthesis, these findings indicate that NagA also has a role in modulating the composition of mycobacterial cell wall AG.

In addition, the nagA deletion strain exhibited a severe defect in biofilm formation (Fig. 6). Although the extracellular polymeric substance composition of mycobacterial biofilms is not yet well-defined, sugar content analyses have identified the presence of mycobacterial cell wall sugars, including the released GlcNAc PG fragment, as integral components of this extracellular matrix (54). Our data indicate that high GlcNAc levels impair the formation of this structure, eliciting fragile biofilms with an altered architecture in WT M. smegmatis, highlighting the importance of nutrient and stress conditions on biofilm structure and composition. As we have established that NagA orchestrates GlcNAc recovery and reuse, we speculate that the formation of disrupted biofilms is linked to an accumulation of GlcNAc within the extracellular matrix combined with $\Delta nagA$'s inability to recycle PG. Since disruption of other enzymes in the mycobacterial PG synthesis pathway also display defective biofilms (38, 39, 55), more work is now needed to unravel the exact role and molecular mechanisms of PG recycling in biofilm establishment and formation.

In conclusion, we have revealed that NagA has a pivotal role in salvaging PG in mycobacteria, providing a specialized pathway for these bacteria to recover scarce energy resources within a nutrient restricted environment. Loss of GlcNAc-6-P deacetylase activity creates a major bottleneck in the recovery of remodeled PG fragments, which leads to reprogramming of amino sugar flux and impedes a myriad of cellular processes. Given NagA's crucial role in cell wall and biofilm formation, the development of NagA inhibitors combined with molecules that exploit the defective cell envelope or exhibit increased efficacy in the presence of defective biofilms could enhance the effectiveness of TB therapy, opening new avenues to explore to combat this major global pathogen.

Experimental procedures

Bacterial strains and culture conditions

M. smegmatis mc²155 strains were routinely cultured aerobically in either Luria-Bertani broth supplemented with 0.05% (vol/vol) Tween 80, Middlebrook 7H9 broth (Difco) supplemented with 0.2% (vol/vol) glycerol and 0.05% (vol/vol) Tween 80 (7H9), Sauton minimal media (0.5 g/L K₂HPO₄, 0.5 g/L MgSO₄, 4.0 g/L asparagine, 2.0 g/L citric acid, 0.05 g/L ferric ammonium citrate, 0.0001% (wt/vol) ZnSO₄ and 0.05% (vol/vol) tyloxapol containing the carbon source of interest supplemented with a defined carbon source at the indicated concentrations or Sauton-glycerol media (Sauton minimal media containing 5% (vol/vol) glycerol). Strains were routinely maintained on LB agar or Middlebrook 7H10 agar (Difco) supplemented with 10% (vol/vol) oleic acid-albumindextrose-catalase and 0.2% glycerol at 37 °C. Hygromycin (50 μg/ml) and kanamycin (25 μg/ml) were used when

required. For growth on defined carbon sources, strains were cultured to mid-log phase and starved for 24 h in PBS supplemented with 0.05% tyloxapol (PBST) before inoculation into Sauton minimal media supplemented with the appropriate carbon source. For cloning procedures E. coli Top10 cells were grown in LB or on LBA supplemented with hygromycin (150 μ g/ml) and kanamycin (50 μ g/ml).

Generation of the nagA gene-deletion mutant

The nagA deletion mutant was achieved using the phage based specialized transduction method. The allelic exchanges substrate for nagA was generated in the digested p0004s vector (a gift from Professor William R. Jacobs Jr, Albert Einstein College of Medicine, USA). Two DNA fragments corresponding to ~ 1000 bases upstream and downstream of nagA were PCR amplified from M. smegmatis genomic DNA using the primers (MSMEG2119_LL, MSMEG2119_LR, MSMEG2119_RL, and MSMEG2119_RR) listed in Table S4. The PCR products were digested with AlwNI and ligated with the hyg^R-sacB cassette and oriE-cos fragments released from the Van91I-digested p0004S vector. The allelic exchange plasmid: nagA_p0004s, was verified by DNA sequencing, using the primer pairs HL/OL and HR/OR (Table S4). The resulting knockout plasmid was linearized with PacI and cloned into phasmid phAE159, as described (56). Allelic exchange in M. smegmatis was achieved by specialized transduction using hygromycin for selection, resulting in the replacement of *nagA* with the $\gamma \delta res$ -sacB-hyg- $\gamma \delta res$ cassette. The M. smegmatis $\Delta nagA$ mutant strain was confirmed by whole-genome sequencing of isolated genomic DNA (MicrobesNG). The sequencing data generated in this study have been deposited in the European Nucleotide Archive (ENA) under the accession number PRJEB90657. The data are available https://www.ebi.ac.uk/ena/browser/view/ PRJEB90657.

Growth point monitoring of M. smegmatis

The growth of M. smegmatis strains in indicated growth media at 37 °C was monitored by measuring the absorbance at 600 nm (A_{600}) at the time points indicated. The M. smegmatis starting A_{600} was 0.05. All experiments were undertaken in triplicate. Data were analyzed in GraphPad Prism (v10.1.1), and statistical significance was determined by Holm-Sídák multiple unpaired t-tests for each experimental group comparing $\Delta nagA$ to the WT control.

NagA activity assay

M. smegmatis cultures were grown in 7H9 broth to an $A_{600} = \sim 1$, washed twice in 0.1 M TES, pH 7.5, sonicated (amplitude = 8, 30 s on, 30 s off, 4 °C (Soniprep 150 Plus Ultrasonic Disintegrator)) and the clarified lysate obtained by centrifugation (16,000g, 10 min, 4 °C). Deacetylase activity in cell lysates was determined as previously described (57). The assay (250 µl) contained clarified lysate (100 µl), 0.2 M sodium phosphate buffer pH 7.5 (50 µl) and final concentrations of 10 mM N-acetylglucosamine-6-phosphate, 2 mM NADP, 4 U



phosphoglucose isomerase, and 1.5 U glucose-6-phosphate dehydrogenase. The cell lysate assay was incubated at 37 °C for 60 min and the rate of formation of NADPH was determined spectrophotometrically at 340 nm (Tecan Infinite M200). Total lysate protein concentration was determined by a Bradford assay (590 nm, Tecan Infinite M200). Kinetic parameters were analyzed by nonlinear regression analysis (GraphPad Prism, v10.1.1) and expressed as mean ± standard deviation of triplicate measurements.

Determination of 14C-GlcNAc uptake

M. smegmatis cells were grown to an $A_{600} = 1$ in Sauton minimal media (100 ml) supplemented with glucose (5 mM), or glucose (5 mM) and GlcNAc (1 mM). The cells were harvested by centrifugation (3220g, 10 min, 4 °C), washed three times in PBST and resuspended in PBST (300 µl) to give an A_{600} of $\sim\!\!266$. Uptake assays were performed at 37 $^{\circ}\mathrm{C}$ with $^{14}\mathrm{C}$ -GlcNAc [glucosamine-14C(U)] (0.01 µCi/ml) (specific activity 250-360 mCi/mmol 9.25-13.32 GBq/mmol, American Radiolabeled Chemicals). Samples (30 µl) were taken at the indicated time points over 30 min. Uptake was terminated at 2.5 min, within the linear range, by the addition of 1 ml icecold PBST containing 500 mM GlcNAc (quenching buffer), followed immediately by centrifugation (16,000g, 10 min, 4 °C). The cell pellets were washed three times in ice-cold quenching buffer (1 ml) and then resuspended in 500 µl of the same buffer. The radioactivity corresponding 14C-GlcNAc uptake in the 500 µl sample was measured by scintillation counting in scintillation fluid (10 ml) (Ecoscint A, National Diagnostics). Each assay was performed in triplicate. ¹⁴C-GlcNAc uptake rates were determined at 2.5 min and expressed as mean ± standard deviation of triplicate measurements.

¹⁴C-GlcNAc labeling

Mid-log phase *M. smegmatis* strains ($A_{600} = \sim 0.5$) were inoculated into Sauton minimal media supplemented with either glucose (5 mM) or glucose (5 mM) and GlcNAc (1 mM) to an absorbance of $A_{600} = 0.1$ before radiolabeling with $\mu Ci/ml$ ¹⁴C-GlcNAc [glucosamine-14C(U)] (250– 360 mCi/mmol 9.25-13.32 GBq/mmol, American Radiolabeled Chemicals) for 20 h at 37 °C. Cells were harvested by centrifugation (3220g, 10 min, 4 °C), washed five times with PBST supplemented with 500 mM GlcNAc and the cell fractions analyzed as described previously (33). Briefly, pellets were boiled in 4% SDS (500 µl) for 3 h, centrifuged (16,000g, 10 min, room temperature) and the supernatant retained as the cytosol sample. The pellet was subjected to boiling in 0.1 M HCl (500 µl) for 30 min to release the AG and GlcNAc containing linker fraction and the supernatant retained as the AG sample after centrifugation (16,000g, 10 min, room temperature). The remaining insoluble material in the pellet represents the peptidoglycan and was resuspended in water (500 μl). Samples (500 μl) were measured for radioactivity by scintillation in scintillation fluid (10 ml) (Ecoscint A, national diagnostics) All assays were performed in triplicate. Data were analyzed in GraphPad Prism (v10.1.1) and statistical significance was determined by Holm-Šídák multiple unpaired t-tests for each experimental group comparing $\Delta nagA$ to the WT control.

Determination of MICs

The MICs of all compounds were determined using the resazurin reduction microplate assay as described previously described (58). Briefly, M. smegmatis strains were grown to mid-log phase ($A_{600} = 0.6$) and approximately 5×10^5 cells were incubated at 37 °C in 7H9 broth containing 2-fold serial dilutions of each compound in a 96-well flat-bottom microtiter plate. The plates were incubated without shaking for 24 h before addition of 25 µl resazurin (one tablet of resazurin (VWR) dissolved in 30 ml of sterile PBS supplemented with 10% (vol/vol) Tween-80). Following a further 3 h incubation at 37 °C, the plates were assessed for color development. The MIC values were determined as the lowest concentration of drug that prevented the color change of resazurin (blue: no bacterial growth) to resorufin (pink: bacterial growth).

Determination of drug susceptibility by spot assays

The percentage recovery of M. smegmatis WT and $\Delta nagA$ strains were determined against the compounds where twofold differences in MIC values determined by resazurin reduction microplate assay were observed. WT and $\Delta nagA$ strains were grown to mid-log phase ($A_{600} = 0.6$). The cells were serially diluted in 7H9 media and spotted (10 μ l) at 10^6 to 10¹ cells/well in 24-well plates containing 7H10 media (1 ml) with or without compound at concentration dilutions around the determined MIC values. The plates were incubated at 37 °C for 48 h, the colony forming units counted and CFU/ml calculated. The relative percentage recovery is expressed as a fraction compared to the CFU/ml of the untreated strains. All assays were performed in triplicate.

Lysozyme susceptibility assay

M. smegmatis strains were grown to early log phase $(A_{600} = 0.25)$ in 7H9 media. In addition, 100 µl of this culture was added to a 96 well-plate with the addition of 200 μg/ml lysozyme (final concentration) and incubated at 37 °C for 3 h, at which point samples were taken for CFU enumeration. The percentage survival was calculated by comparison to CFUs from a no lysozyme control. All assays were carried out in triplicate. Data were analyzed in GraphPad Prism (v10.1.1), and statistical significance was determined by a two-tailed t test.

Ethidium bromide uptake

Mid-log phase *M. smegmatis* cultures ($A_{600} = 0.5$) grown in 7H9 broth were harvested by centrifugation (3220×g, 10 min, 4 °C), washed in PBST and resuspended in PBST to an A_{600} = 0.8. Uptake assays were performed with 100 µl cell suspension and a final concentration of 2 μg/ml ethidium bromide and the fluorescence monitored at λ_{ex} 535 nm, λ_{em} 595 nm (Tecan Infinite F200). Samples were taken every 10 min for a period of 60 min. The change in fluorescence was calculated by subtracting the fluorescence at time = 0 from the end point time = 60 min. Ethidium bromide uptake assays were carried out in triplicate. Data were analyzed in the Superviolin package in Python 3 (Minicondia), and statistical significance was determined by a two-tailed t test.

Congo red binding

M. smegmatis strains (5 ml) were grown in triplicate for 3 days at 37 °C in 7H9 broth and 100 μg/ml congo red before harvesting (3220g, 10 min, 4 °C). The cells were then washed at least 5 times with water (10 ml) until the supernatant became clear. The pelleted cells were resuspended in water (1 ml), the A_{600} determined, and the cells then pelleted by centrifugation (3220g, 10 min, 4 °C). The cells were then incubated with dimethyl sulfoxide (1 ml) for 4 h at room temperature, with shaking. The cells were then pelleted (3220g, 10 min, 4 °C), and the absorbance of the dimethyl sulfoxide extract measure at 488 nm (A488). The Congo red binding index was calculated as a measure of A488 divided by the A_{600} . All assays were performed in triplicate. Data were analyzed in GraphPad Prism (v10.1.1), and statistical significance was determined by a two-tailed t test.

Growth conditions for peptidoglycan extraction, flow cytometry analysis, and transmission electron microscopy

M. smegmatis strains were grown to exponential phase $(A_{600} \approx 1.2)$ in LB media containing 0.05% Tween 80 (100 ml). The cells were harvested by centrifugation (3220g, 10 min, 4 °C), washed three times in PBST, and the pelleted cells resuspended in PBST (100 ml). The cells were then starved for 24 h at 37 °C with shaking, centrifuged (3220g, 10 min, 4 °C), resuspended in Sauton minimal media and inoculated into Sauton minimal media supplemented with either glucose (5 mM) or glucose (5 mM) and GlcNAc (1 mM) to an absorbance of $A_{600} = 0.05$. The cells were grown to either mid-log ($A_{600} = \sim 0.6$) or stationary phase (48 h, $A_{600} = \sim 1.3$), centrifuged (3220g, 10 min, 4 °C) and washed three times in PBST and the cell pellet retained for either PG extraction, imaging flow cytometry analysis or TEM.

Peptidoglycan extraction

Cell pellets from 3 × 1L were resuspended in PBS (10 ml per 1L pellet) and lysed by sonication on ice $(10 \times 30 \text{ s on}, 30 \text{ s})$ off, Sonicator Ultrasonic Liquid Processor XL; Misonix). The lysates were combined and then subjected to boiling in 4% SDS to release the mAGP complex, and the insoluble mAGP collected by centrifugation (20,000g, 30 min, room temperature) and washed 10 times with water (35 ml) to remove the SDS (20,000g, 20 min, room temperature). The isolated mAGP was then resuspended in 0.5% (w/v) KOH in methanol and incubated at 37 °C for 96 h at 180 rpm to cleave the mycolic acids. The insoluble material containing the cleaved mycolic acids and the arabinogalactan-peptidoglycan complex was collected by centrifugation (3220g, 10 min, room temperature) and washed three times with methanol (15 ml) to remove the KOH. The cleaved mycolic acids were extracted from the mixture by washing three times with diethyl ether (15 ml, 3220g, 10 min, room temperature). The resulting arabinogalactan-peptidoglycan complex was then treated with 0.2 M H₂SO₄ at 85 °C for 30 min (without shaking) to release the AG. The mixture was then cooled and neutralized with NaHCO₃. The insoluble PG was separated from the solubilized AG by centrifugation (3220g, 10 min, room temperature), washed with water three times, resuspended in 1 ml PBS (1 ml) and treated with DNase (20 mg/ml) and RNase (10 mg/ml) and incubated at 37 °C for 4 h at 600 rpm, before adding proteinase K (100 mg/ml) and incubated at 55 °C for 16 h, 600 rpm. SDS was then added to give a final concentration of 1% (wt/vol) and the samples boiled for 3 h before harvesting the PG by centrifugation (3220g, 10 min, room temperature) and washing the isolated PG with water 10 times (10 ml) to remove the SDS. The isolated PG samples were lyophilized and stored at −20 °C.

Peptidoglycan digestion

One milligram of purified peptidoglycan was resuspended in 20 mM phosphate buffer, pH 5.5 (125 µl) supplemented with 200 U of mutanolysin (Sigma-Aldrich) and digested for 16 h, at 37 °C with agitation. Following heat inactivation of mutanolysin (5 min at 100 °C), soluble disaccharide peptides were mixed with an equal volume of 250 mM borate buffer (pH 9.25) and reduced with 0.2% (wt/vol) sodium borohydride for 20 min at room temperature, and the pH was then adjusted to 4.5 to 5.5 with phosphoric acid.

LC-MS/MS data acquisition

An Ultimate 3000 UHPLC (Dionex) system coupled with a high-resolution Q Exactive Focus mass spectrometer (Thermo Fisher Scientific) was used for LC-MS/MS analysis. Muropeptides were separated using a C18 column (Hypersil Gold aQ, 1.9 μm particles, 150 mm × 2.1 mm; Thermo Fisher Scientific) at a temperature of 50 °C. Muropeptide elution was performed at 0.25 ml/min with mixture of solvent A (water, 0.1% [vol/vol] formic acid) and solvent B (acetonitrile, 0.1% [vol/vol] formic acid). LC conditions were 0 to 12.5% B for 25 min increasing to 20% B for 10 min. After 5 min at 95%, the column was re-equilibrated for 10 min with 100% buffer A. The Orbitrap Exploris 240 was operated under electrospray ionization (H-ESI high flow)-positive mode, full scan (m/z 150-2250) at resolution 120,000 (FWHM) at m/z 200, with normalized AGC Target 100%, and automated maximum ion injection time (IT). Data-dependent MS/MS were acquired on a 'Top 5' data-dependent mode using the following parameters: resolution 30,000; AGC 100%, automated IT, with normalized collision energy 25%.

LC-MS/MS data analysis strategy

A preliminary search was carried out to identify disaccharide-peptides present across all datasets using the proprietary software Byos. We searched LC-MS/MS datasets using a database containing 156 muropeptides (DB1; Supplementary File S1) including di, tri, tetra and pentapeptide



stems containing A, E, Q, m-DAP (amidated or not) and noncanonical residues at their C terminus. These peptide stems were searched with N-terminal modifications corresponding to various disaccharide-peptides including GlcNAc-MurNAc (gm) as well as their glycolylated (gm(Glyc) and deacetylated variants gm(DeAc). The automated MS/MS analysis did not identify any noncanonical residues. It confirmed the presence of glycolylated MurNAc and deacetylated sugar residues, as well as the presence of peptide stems containing Glu or Gln and both m-DAP (referred to as J) and amidated m-DAP (referred to as Z). Using this information, we next built a database containing 24 monomers (DB2; Supplementary File S1) containing the gm(Glyc) and gm disaccharides moieties linked to peptide stems containing A,E, Q,J and Z (AEJAA, AQJAA, AEZAA, and AQZAA). DB2 was used to perform searches using the open-source software PGFinder (59, 60). Datasets were deconvoluted using Byos, and searches were carried out using a 5 ppm tolerance, allowing the search for deacetylated variants. A total of 29 monomers (including eight deacetylated ones) were identified across all samples (Supplementary File S2). The search output was chosen to identify the eight most abundant monomers that could be used as a donor or an acceptor (gm-AEJ, gm-AEJA, gm(Glyc)-AEZ, gm(Glyc)-AEZA, gm(Glyc)-AEJ, gm (Glyc)-AEJA, gm(Glyc)-AQZ, and gm(Glyc)-AQZA). These eight muropeptides were used to build 64 dimers. A total of 20 dimers were identified across all samples. All monomers from DB2, the eight deacetylated monomers identified by PGFinder and the 64 dimers built were combined to generate a final database called DB3 (Supplementary File S1). DB3 was used for a "one off" search (Supplementary File S3).

Determination of cell size by flow cytometry

Cell pellets were washed once with PBST and resuspended in PBST to an A_{600} of 0.2. Samples were imaged using multispectral imaging flow cytometry (CYTEK ImageStream^X MkII, Amnis Corporation) acquiring 30,000 events per sample across three biological repeats. Imaging was performed using the 60× magnification lens, with the 488 nm laser (100 mW) for brightfield channel imaging. Data were analyzed using IDEAS software (IDEAS v6.3, Amnis Corporation). Single rod-shaped cells were gated based on the "area" versus aspect ratio plot of the brightfield image (aspect ratio: cell minor axis divided by cell major axis). After gating \sim 10,000 single rod-shaped WT cells and \sim 10,000 Δ nagA cells were measured. Cells were masked using the "Adaptive Erode" mask with a 74-pixel threshold. This cutoff was selected as the highest threshold that masked the cell (Fig. S11). Cell length was derived from this mask using the "length" feature. Data were analyzed in GraphPad Prism (v10.1.1), and statistical significance determined by an unpaired t test.

Analysis of cells by TEM

Cell pellets were resuspended in PBS containing 2.5% glutaraldehyde and incubated at room temperature for 1 h, centrifuged (10 min, 3220g, 4 °C), washed once with PBST and washed three times in water. The cells were resuspended in 1% (wt/vol) osmium tetroxide for 1 h to stain and then washed. After stepwise dehydration in 25%, 50%, 75%, and 100% (vol/vol) acetone, the cells were infiltrated with 50% (wt/vol) resin (Agar LV resin) for 1 h followed by 100% resin for 24 h. The Agar LV resin was cured at 60 °C overnight. After ultrathin sectioning on an RMC ultramicrotome, sections were post stained in 2% (wt/vol) uranyl acetate and 1.5% (wt/vol) lead citrate. The samples were imaged in a JEOL JEM2100Plus with Gatan OneView CMOS camera. Images were processed in ImageJ using the "plot profile" feature.

Metabolite analysis by ion chromatography

Strains were cultured in Sauton-glycerol media (200 ml) to $A_{600} = \sim 1.0$ with or without the addition of GlcNAc (20 mM). Cells were harvested by centrifugation (3220g, 10 min, 4 °C), washed with PBST twice, snap frozen, resuspended in water, lysed by sonication (amplitude = 8, 30 s on, 30 s off, 4 °C, Soniprep 150 Plus Ultrasonic Disintegrator) and centrifuged (16,000g, 10 min, 4 °C). The supernatant was lyophilized before resuspension in 500 μ l 18 M Ω H₂O, filtered through a 10-kDa molecular weight cutoff centrifuge filter (Amicon) and the filtrate analyzed. Samples were analyzed by highperformance anion-exchange chromatography on a Dionex ICS5000+ system with a CarboPac PA-20 analytical column $(3 \text{ mm} \times 150 \text{ mm})$ and PA-20 guard column $(3 \text{ mm} \times 30 \text{ mm})$ kept at 30 °C. Detection was by pulsed amperometry with standard quadrupole waveform. Multistep gradient elution was performed as shown in Table 2 (eluent A = 18.2 M Ω H₂O,

Table 2 High-performance anion-exchange chromatography KOH elution gradient

| Time (mins) | % Eluent A (H ₂ O) | % Eluent B (100 mM NaOH) | % Eluent C: (100 mM NaOH-800 mM NaOAc) | Flow rate (mL/min) |
|-------------|-------------------------------|--------------------------|--|--------------------|
| 0 | 95 | 5 | 0 | 0.5 |
| 5 | 95 | 5 | 0 | 0.5 |
| 20 | 50 | 50 | 0 | 0.5 |
| 35 | 50 | 25 | 25 | 0.5 |
| 40 | 50 | 25 | 25 | 0.5 |
| 41 | 50 | 50 | 0 | 0.5 |
| 43 | 95 | 5 | 0 | 0.5 |
| 50 | 95 | 5 | 0 | 0.5 |

eluent B = 100 mM NaOH, eluent C = 100 mM NaOH, 800 mM NaOAc) with a total run time of 50 min. Authentic standards of N-acetylglucosamine, N-acetylglucosamine-6phosphate, glucosamine-6-phosphate were run for comparison. Chromeleon 7 software (Dionex) was used for data processing. To quantify uptake, the peak area of the GlcNAc, GlcNAc-6-P, and GlcN-6-P standards at varying concentrations (GlcN: 0-10 μM, GlcNAc: 0-25 μM, GlcN-6-P: 0-100 μM, GlcNAc-6-P 0–100 μM) were measured (Chromeleon 7 software). The peak area was plotted against concentration and simple linear regression plotted. To determine the concentration of these metabolites in cytosolic samples, the area of the peaks of interest was measured (Chromeleon 7 software) and the concentration determined from the calibration plot. Data were analyzed in GraphPad Prism (v10.1.1), and the statistical significance was determined by Holm-Sídák multiple unpaired t-tests for each experimental group comparing $\Delta nagA$ to the WT control.

Biofilm generation and quantification

M. smegmatis strains were cultured in Sauton-glycerol media supplemented with 0.05% Tween-80 at 37 °C, with shaking to mid-log phase ($A_{600} = 0.6$). Cultures were diluted to $A_{600} = 0.03$ in detergent free Sauton-glycerol medium with or without 20 mM GlcNAc and seeded into 24 or 96 well plates. Pellicles were incubated without shaking at 30 °C for 7 days before imaging, biofilm quantification and CFU enumeration. Crystal violet assays were performed to quantify biofilm biomass. Media were removed from the well, and the remaining biofilm was dried at 37 °C and stained with crystal violet (1 ml 0.1% (wt/vol) crystal violet solution). After 15 min incubation at room temperature the wells were washed with water (3 × 1 ml) and crystal violet extracted in ethanol (1 ml) followed by measurement of the absorbance of the solution at 600 nm (Tecan Infinite M200). CFUs were determined from biofilms cultured in 96-well plates by the addition of Tween-80 to a final concentration of 0.1% to each well and incubation for 30 min at room temperature before homogenizing the biofilm by pipetting. Wells were incubated for a further 10 min at room temperature before repeating homogenizing by pipetting. The solution was 10-fold serially diluted, the dilutions plated onto LBA, incubated at 37 °C for 3 days and CFUs determined. All assays were performed in triplicate. Data were analyzed in GraphPad Prism (v10.1.1) and statistical significance was determined by Holm-Sídák multiple unpaired t-tests for each experimental group comparing Δ *nagA* to the WT control.

Proteomic sample preparation and analysis

M. smegmatis strains (WT and Δ nagA, 30 ml) were grown to an A_{600} of 0.8 in 7H9 media. The cells were harvested (3550g, 20 min, 4 °C), washed (3 × PBST) and the pellet resuspended in lysis buffer (PBS, 1 mM DTT, 1 mg/ml lysozyme, protease inhibitor (Pierce) pH 7.4) for 2 h at room temperature. 0.1 mm silica glass beads were added, and the cells were disrupted by bead-beating (4 × 45 s on, 45 s off, placed on ice between

cycles, 6 m/sec, FastPrep-24 5G (MP Biomedicals)) followed by sonication (water sonicator bath) at room temperature for 15 min. The samples were centrifuged (2300g, 20 min, 4 °C) and the supernatant collected. The protein concentration was determined by Qubit fluorometer (Invitrogen) using Qubit Protein Assay Kit (Invitrogen). Protein samples (15 µl) were mixed with 2 × SDS loading dye, loaded directly onto an SDSgel (Bio-Rad Any kD Mini-PROTEAN TGX) and run for 5 min, and the excised gel bands prepared for proteomics analysis as described previously (61). In brief, samples were reduced with 10 mM tris-2(-carboxyethyl)-phosphine (TCEP), alkylated with 40 mM chloroacetamide (CAA) and then in-gel digested with trypsin (2.5 ng/ml), and the peptides extracted with 25% acetonitrile containing 5% formic acid. The extracted peptides were dried under vacuum to a volume of 20 µl and resuspended to a total volume of 50 µl in 2% acetonitrile, 0.1% trifluoroacetic acid. Mass spectrometry was performed on a Thermo Orbitrap Fusion (Thermo Fisher Scientific) coupled to an Ultimate 3000 RSLCnano HPLC (Dionex) using an Acclaim PepMap μ -precolumn cartridge (300 μ m i.d. \times 5 mm, 5 μ m, 100 Å) and an analytical Acclaim PepMap RSLC column (75 μ m i.d. × 50 cm, 2 μ m, 100 Å, Thermo Fisher Scientific). Mobile phase buffer A was composed of 0.1% (vol/vol) formic acid in water, and mobile phase B was composed of acetonitrile containing 0.1% (vol/vol) formic acid. The gradient was programmed as follows: 4% B increased to 25% B over 90 min, then further increased to 35% B over 13 min, followed by 3 min 90% B with a flow rate of 250 nl/min. Survey scans of peptide precursors from 375 to 1575 m/z were performed at 120 K resolution (at 200 m/z) with a 2 × 10⁵ ion count target. The maximum IT was set to 150 ms. Tandem MS was performed by isolation at 1.2 Th using the quadrupole, higher-energy collisional dissociation fragmentation with normalized collision energy of 33, and rapid scan MS analysis in the ion trap. The MS^2 ion count target was set to 3×10^3 and maximum IT was 200 ms. Precursors with charge state 2 to 6 were selected and sampled for MS². The dynamic exclusion duration was set to 45 s with a 10 ppm tolerance around the selected precursor and its isotopes. Monoisotopic precursor selection was turned on and instrument was run in top speed mode. The raw data were searched using MaxQuant with an integrated Andromeda search engine (V1.5.5.1) (62) against both the M. smegmatis database and the common contaminant database from Max-Quant. Peptides were generated from a tryptic digestion with up to two missed cleavages, carbamidomethylation of cysteines as fixed modifications, and oxidation of methionines as variable modifications. Precursor mass tolerance was 10 ppm and product ions were searched at 0.8 Da tolerances. For protein quantification, label-free quantification (LFQ) was selected and proteins with LFQ minimum ratio count of two were retained. The PSM false discovery rate (FDR), protein FDR and site decoy fraction were set to one for further analysis in Scaffold or to 0.01 for analysis in Perseus. Scaffold (version 4.6.2) was used to validate MS/MS based peptide and protein identifications. Peptide identifications were accepted if they could be established at greater than 95.0% probability by the Scaffold Local FDR algorithm. Protein identifications were accepted if they



could be established at greater than 95.0% probability and contained at least two identified peptides. Proteins that contained similar peptides and could not be differentiated based on MS/MS analysis alone were grouped to satisfy the principles of parsimony. Proteins sharing significant peptide evidence were grouped into cluster. Data processing and annotation was performed used the Perseus module of MaxQuant version 1.6.2.2 (63). First, the reverse and contaminant hits (as defined in MaxQuant) were eliminated from the MaxQuant output files. Only protein groups identified with at least two uniquely assigned peptide and quantified with a minimum of two ratio counts were used for the analysis. For each experiment, the LFQ intensity was transformed using the binary logarithm (log₂). Protein groups were considered reproducibly quantified if identified and quantified in at least two replicates, missing LFQ intensity scores were assigned from a normal distribution. Protein groups were assigned a probability value (p-value) using a two-sample Student's t test. p-values were subject to a -log₁₀ transformation. Proteins were considered significant if the p-value < 0.05 ($-\log_{10}(p\text{-value})$ greater than 1.30) and had a two-fold change in protein expression (log₂(LFQ difference) greater than one or <-1). Protein function, product, functional category were assigned based on Mycobrowser (release 3) annotations (64). The mass spectrometry proteomics data have been deposited to the ProteomeXchange Consortium via the PRIDE partner repository with the dataset identifier PXD065120 and 10.6019/PXD065120.

Data availability

All the data generated in this study can be shared upon request.

Supporting information—This article contains supporting information.

Acknowledgments—We thank Professor William R. Jacobs Jr. (Albert Einstein College of Medicine, USA) for providing the phage transduction reagents. We thank Chris de Wolf for assistance with ion chromatography analyses. We acknowledge equipment access, training and support made available by the Warwick Integrative Synthetic Biology centre (WISB) and the Warwick Advanced Bioimaging Research Technology Platform.

Author contributions—C. S. G., C. C., M. K., J. H., A. S., L. S. S. G., C. A. E., S. E. B., A. Bottrill., S. M., and E. F. investigation; C. S. G., C. C., M. K., J. H., L. S. S. G., S. E. B., A. Bottrill., S. M., and E. F. formal analysis; C. S. G., C. C., M. K., J. H., L. S. S. G., S. M., and E. F. visualization; C. S. G., C. C., M. K., J. H., L. S. S. G., S. E. B., A. Bottrill., A. Bhatt., S. M., G. S. B., and E. F. writing—review and editing; C. S. G., C. C., M. K., J. H., S. M., and E. F. writing—original draft; C. S. G., A. S., A. Bottrill., A. Bhatt., G. S. B., and E. F. supervision; A. Bottrill., A. Bhatt. S. M., and G. S.B. resources; S. M., G. S. B., and E. F. funding acquisition; E. F. conceptualization; E. F. project administration.

Funding and additional information—This work was supported by a Sir Henry Dale Fellowship to E. F. jointly funded by the Wellcome Trust and Royal Society (104193/Z/14/Z and 104193/Z/14/B),

research grants from the Royal Society (RG120405) and the Leverhulme Trust (RPG2019087) and the BBSRC for a studentship to M. K. (BB/M01116X/1). G. S. B. acknowledges support in the form of a Personal Research Chair from Mr James Bardrick and the Medical Research Council (MR/S000542/1 and MR/R001154/1). Work in SM lab is funded by a BBSRC grant (BB/W013800/1). The Warwick Integrative Synthetic Biology Centre (WISB) received funding from EPSRC and BBSRC (BB/M017982/1 and BB/X019411/1) and the Warwick Advanced Bioimaging Research Technology Platform (JEOL 2100Plus) received funding from the MRC (MC_PC_17136) and EPSRC (EP/V007688/1). Genome sequencing was provided by MicrobesNG (http://www.microbesng.uk) supported by the BBSRC (BB/L024209/1).

Conflict of interest—The authors declare that they have no conflicts of interest with the contents of this article.

Abbreviations—The abbreviations used are: AG, arabinogalactan; CFU, colony forming unit; EDL, electron dense layer; FDR, false discovery rate; GlcN-6-P, glucosamine-6-phosphate; IT, injection time; LC-MS/MS, liquid chromatography-tandem mass spectrometry; LFQ, label-free quantification; MIC, minimum inhibitory concentration; Mtb, *Mycobacterium tuberculosis*; PBST, PBS supplemented with 0.05% tyloxapol; PG, peptidoglycan; PTS, phosphotransferase system; TB, tuberculosis; TEM, transmission electron microscopy.

References

- 1. Paulson, T. (2013) Epidemiology: a mortal foe. Nature 502, S2-S3
- Migliori, G. B., Tiberi, S., Zumla, A., Petersen, E., Chakaya, J. M., Wejse, C., et al. (2020) MDR/XDR-TB management of patients and contacts: challenges facing the new decade. The 2020 clinical update by the Global Tuberculosis Network. Int. J. Infect. Dis. 92S, S15–S25
- 3. Abrahams, K. A., and Besra, G. S. (2018) Mycobacterial cell wall biosynthesis: a multifaceted antibiotic target. *Parasitology* **145**, 116–133
- Brennan, P. J., and Nikaido, H. (1995) The envelope of mycobacteria. *Annu. Rev. Biochem.* 64, 29–63
- Jackson, M. (2014) The mycobacterial cell envelope-lipids. Cold Spring Harb Perspect. Med. 4, a021105
- Mahapatra, S., Crick, D. C., and Brennan, P. J. (2000) Comparison of the UDP-N-acetylmuramate:L-alanine ligase enzymes from Mycobacterium tuberculosis and Mycobacterium leprae. J. Bacteriol. 182, 6827–6830
- Mahapatra, S., Crick, D. C., McNeil, M. R., and Brennan, P. J. (2008) Unique structural features of the peptidoglycan of Mycobacterium leprae. J. Bacteriol. 190, 655–661
- Harrison, J. L. G., Joe, M., Lowary, T. L., Reynolds, E., Walters-Morgan, H., Bhatt, A., et al. (2016) Lcp1 is a phosphotransferase responsible for ligating arabinogalactan to peptidoglycan in Mycobacterium tuberculosis. mBio 7. https://doi.org/10.1128/mbio.00972-16. e00972-16
- Alderwick, L. J., Harrison, J., Lloyd, G. S., and Birch, H. L. (2015) The mycobacterial cell Wall–Peptidoglycan and Arabinogalactan. *Cold Spring Harb Perspect. Med.* 5, a021113
- Li, S., Kang, J., Yu, W., Zhou, Y., Zhang, W., Xin, Y., et al. (2012) Identification of M. tuberculosis Rv3441c and M. smegmatis MSMEG_1556 and essentiality of M. smegmatis MSMEG_1556. PloS One 7, e42769
- Moraes, G. L., Gomes, G. C., Monteiro de Sousa, P. R., Alves, C. N., Govender, T., Kruger, H. G., et al. (2015) Structural and functional features of enzymes of Mycobacterium tuberculosis peptidoglycan biosynthesis as targets for drug development. Tuberculosis (Edinb) 95, 95–111
- 12. Ahangar, M. S., Furze, C. M., Guy, C. S., Cooper, C., Maskew, K. S., Graham, B., et al. (2018) Structural and functional determination of



- homologs of the Mycobacterium tuberculosis N-acetylglucosamine-6phosphate deacetylase (NagA). J. Biol. Chem. 293, 9770-9783
- 13. Karlikowska, M., Singh, A., Bhatt, A., Ott, S., Bottrill, A. R., Besra, G. S., et al. (2021) Biochemical and phenotypic characterisation of the Mycobacterium smegmatis transporter UspABC. Cell Surf. 7, 100052
- 14. Cole, S. T., Brosch, R., Parkhill, J., Garnier, T., Churcher, C., Harris, D., et al. (1998) Deciphering the biology of Mycobacterium tuberculosis from the complete genome sequence. Nature 393, 537-544
- 15. Craggs, P. D., Mouilleron, S., Rejzek, M., de Chiara, C., Young, R. J., Field, R. A., et al. (2018) The mechanism of acetyl transfer catalyzed by Mycobacterium tuberculosis GlmU. Biochemistry 57, 3387-3401
- 16. Li, Y., Zhou, Y., Ma, Y., and Li, X. (2011) Design and synthesis of novel cell wall inhibitors of Mycobacterium tuberculosis GlmM and GlmU. Carbohydr. Res. 346, 1714-1720
- 17. Verma, S. K., Jaiswal, M., Kumar, N., Parikh, A., Nandicoori, V. K., and Prakash, B. (2009) Structure of N-acetylglucosamine-1-phosphate uridyltransferase (GlmU) from Mycobacterium tuberculosis in a cubic space group. Acta Crystallogr. Sect F Struct. Biol. Cryst. Commun. 65, 435-439
- 18. Gaugue, I., Oberto, J., Putzer, H., and Plumbridge, J. (2013) The use of amino sugars by bacillus subtilis: presence of a unique operon for the catabolism of glucosamine. PloS One 8, e63025
- 19. Park, J. T. (2001) Identification of a dedicated recycling pathway for anhydro-N-acetylmuramic acid and N-acetylglucosamine derived from Escherichia coli cell wall murein. J. Bacteriol. 183, 3842-3847
- 20. Plumbridge, J. (2009) An alternative route for recycling of N-acetylglucosamine from peptidoglycan involves the N-acetylglucosamine phosphotransferase system in Escherichia coli. J. Bacteriol. 191, 5641-5647
- 21. Popowska, M., Osinska, M., and Rzeczkowska, M. (2012) N-acetylglucosamine-6-phosphate deacetylase (NagA) of Listeria monocytogenes EGD, an essential enzyme for the metabolism and recycling of amino sugars. Arch. Microbiol. 194, 255-268
- 22. Rigali, S., Nothaft, H., Noens, E. E., Schlicht, M., Colson, S., Muller, M., et al. (2006) The sugar phosphotransferase system of Streptomyces coelicolor is regulated by the GntR-family regulator DasR and links Nacetylglucosamine metabolism to the control of development. Mol. Microbiol. **61**, 1237–1251
- 23. Rigali, S., Titgemeyer, F., Barends, S., Mulder, S., Thomae, A. W., Hopwood, D. A., et al. (2008) Feast or famine: the global regulator DasR links nutrient stress to antibiotic production by streptomyces. EMBO
- 24. Swiatek, M. A., Tenconi, E., Rigali, S., and andvan Wezel, G. P. (2012) Functional analysis of the N-acetylglucosamine metabolic genes of Streptomyces coelicolor and role in control of development and antibiotic production. J. Bacteriol. 194, 1136-1144
- 25. White, R. J. (1968) Control of amino sugar metabolism in Escherichia coli and isolation of mutants unable to degrade amino sugars. Biochem. J. **106**, 847-858
- 26. Yadav, V., Panilaitis, B., Shi, H., Numuta, K., Lee, K., and Kaplan, D. L. (2011) N-acetylglucosamine 6-phosphate deacetylase (nagA) is required for N-acetyl glucosamine assimilation in Gluconacetobacter xylinus. PloS One 6, e18099
- 27. Aldridge, B. B., Fernandez-Suarez, M., Heller, D., Ambravaneswaran, V., Irimia, D., Toner, M., et al. (2012) Asymmetry and aging of mycobacterial cells lead to variable growth and antibiotic susceptibility. Science **335**. 100-104
- 28. Hansen, J. M., Golchin, S. A., Veyrier, F. J., Domenech, P., Boneca, I. G., Azad, A. K., et al. (2014) N-glycolylated peptidoglycan contributes to the immunogenicity but not pathogenicity of Mycobacterium tuberculosis. J. Infect. Dis. 209, 1045-1054
- 29. Maitra, A., Munshi, T., Healy, J., Martin, L. T., Vollmer, W., Keep, N. H., et al. (2019) Cell wall peptidoglycan in mycobacterium tuberculosis: an achilles' heel for the TB-causing pathogen. FEMS Microbiol. Rev. 43,
- 30. Rosser, A., Stover, C., Pareek, M., and Mukamolova, G. V. (2017) Resuscitation-promoting factors are important determinants of the pathophysiology in Mycobacterium tuberculosis infection. Crit. Rev. Microbiol. 43, 621-630

- 31. Kruh, N. A., Troudt, J., Izzo, A., Prenni, J., and Dobos, K. M. (2010) Portrait of a pathogen: the Mycobacterium tuberculosis proteome in vivo. PloS One 5, e13938
- 32. Cole, S. T., Eiglmeier, K., Parkhill, J., James, K. D., Thomson, N. R., Wheeler, P. R., et al. (2001) Massive gene decay in the leprosy bacillus. Nature **409**, 1007–1011
- 33. Hancock, I. C., Carman, S., Besra, G. S., Brennan, P. J., and Waite, E. (2002) Ligation of arabinogalactan to peptidoglycan in the cell wall of Mycobacterium smegmatis requires concomitant synthesis of the two wall polymers. Microbiology 148, 3059-3067
- 34. Vollmer, W., Blanot, D., and andde Pedro, M. A. (2008) Peptidoglycan structure and architecture. FEMS Microbiol. Rev. 32, 149-167
- 35. Dahl, J. L. (2004) Electron microscopy analysis of Mycobacterium tuberculosis cell division. FEMS Microbiol. Lett. 240, 15-20
- 36. Paul, T. R., and Beveridge, T. J. (1992) Reevaluation of envelope profiles and cytoplasmic ultrastructure of mycobacteria processed by conventional embedding and freeze-substitution protocols. J. Bacteriol. 174, 6508-6517
- 37. Takade, A., Umeda, A., Matsuoka, M., Yoshida, S., Nakamura, M., and Amako, K. (2003) Comparative studies of the cell structures of Mycobacterium leprae and M. tuberculosis using the electron microscopy freeze-substitution technique. Microbiol. Immunol. 47, 265-270
- 38. Di Somma, A., Caterino, M., Soni, V., Agarwal, M., di Pasquale, P., Zanetti, S., et al. (2019) The bifunctional protein GlmU is a key factor in biofilm formation induced by alkylating stress in Mycobacterium smegmatis. Res. Microbiol. 170, 171-181
- 39. Kang, J., Xu, L., Yang, S., Yu, W., Liu, S., Xin, Y., et al. (2013) Effect of phosphoglucosamine mutase on biofilm formation and antimicrobial susceptibilities in M. smegmatis glmM gene knockdown strain. PloS One **8**, e61589
- 40. McNeil, M., Daffe, M., and Brennan, P. J. (1990) Evidence for the nature of the link between the arabinogalactan and peptidoglycan of mycobacterial cell walls. J. Biol. Chem. 265, 18200-18206
- 41. Baranowski, C., Welsh, M. A., Sham, L. T., Eskandarian, H. A., Lim, H. C., Kieser, K. J., et al. (2018) Maturing Mycobacterium smegmatis peptidoglycan requires non-canonical crosslinks to maintain shape. Elife 7. https://doi.org/10.7554/eLife.37516
- 42. Kalscheuer, R., Syson, K., Veeraraghavan, U., Weinrick, B., Biermann, K. E., Liu, Z., et al. (2010) Self-poisoning of Mycobacterium tuberculosis by targeting GlgE in an alpha-glucan pathway. Nat. Chem. Biol. 6, 376-384
- 43. Belisle, J. T., Vissa, V. D., Sievert, T., Takayama, K., Brennan, P. J., and Besra, G. S. (1997) Role of the major antigen of Mycobacterium tuberculosis in cell wall biogenesis. Science 276, 1420-1422
- 44. Johnson, J. W., Fisher, J. F., and Mobashery, S. (2013) Bacterial cell-wall recycling. Ann. N. Y. Acad. Sci. 1277, 54-75
- 45. Machowski, E. E., Senzani, S., Ealand, C., and Kana, B. D. (2014) Comparative genomics for mycobacterial peptidoglycan remodelling enzymes reveals extensive genetic multiplicity. BMC Microbiol. 14, 75
- 46. Khatri, B., Fielder, M., Jones, G., Newell, W., Abu-Oun, M., and Wheeler, P. R. (2013) High throughput phenotypic analysis of Mycobacterium tuberculosis and Mycobacterium bovis strains' metabolism using biolog phenotype microarrays. PloS One 8, e52673
- 47. Titgemeyer, F., Amon, J., Parche, S., Mahfoud, M., Bail, J., Schlicht, M., et al. (2007) A genomic view of sugar transport in Mycobacterium smegmatis and Mycobacterium tuberculosis. J. Bacteriol. 189, 5903-5915
- 48. Fullam, E., Prokes, I., Futterer, K., and Besra, G. S. (2016) Structural and functional analysis of the solute-binding protein UspC from Mycobacterium tuberculosis that is specific for amino sugars. Open Biol. 6, 160105
- 49. Niederweis, M. (2008) Nutrient acquisition by mycobacteria. Microbiology 154, 679-692
- 50. Bernheim, N. J., and Dobrogosz, W. J. (1970) Amino sugar sensitivity in Escherichia coli mutants unable to grow on N-acetylglucosamine. J. Bacteriol. 101, 384–391
- 51. Plumbridge, J. A. (1990) Induction of the nag regulon of Escherichia coli by N-acetylglucosamine and glucosamine: role of the cyclic AMPcatabolite activator protein complex in expression of the regulon. J. Bacteriol. 172, 2728-2735



- 52. Swiatek, M. A., Urem, M., Tenconi, E., Rigali, S., and andvan Wezel, G. P. (2012) Engineering of N-acetylglucosamine metabolism for improved antibiotic production in Streptomyces coelicolor A3(2) and an unsuspected role of NagA in glucosamine metabolism. Bioengineered 3,
- 53. Mills, J. A., Motichka, K., Jucker, M., Wu, H. P., Uhlik, B. C., Stern, R. J., et al. (2004) Inactivation of the mycobacterial rhamnosyltransferase, which is needed for the formation of the arabinogalactan-peptidoglycan linker, leads to irreversible loss of viability. J. Biol. Chem. 279, 43540-43546
- 54. Belardinelli, J. M., Li, W., Avanzi, C., Angala, S. K., Lian, E., Wiersma, C. J., et al. (2021) Unique features of Mycobacterium abscessus biofilms formed in synthetic cystic fibrosis Medium. Front. Microbiol. 12, 743126
- 55. Wang, C., Zhang, Q., Tang, X., An, Y., Li, S., Xu, H., et al. (2019) Effects of CwlM on autolysis and biofilm formation in Mycobacterium tuberculosis and Mycobacterium smegmatis. Int. J. Med. Microbiol. 309, 73-83
- 56. Bardarov, S., Bardarov, S., Pavelka, M. S., Sambandamurthy, V., Larsen, M., Tufariello, J., et al. (2002) Specialized transduction: an efficient method for generating marked and unmarked targeted gene disruptions in Mycobacterium tuberculosis, M. bovis BCG and M. smegmatis. Microbiology 148, 3007-3017
- 57. Homer, K. A., Patel, R., and Beighton, D. (1993) Effects of N-acetylglucosamine on carbohydrate fermentation by Streptococcus mutans NCTC 10449 and Streptococcus sobrinus SL-1. Infect. Immun. 61, 295-302

- 58. Palomino, J. C., Martin, A., Camacho, M., Guerra, H., Swings, J., and Portaels, F. (2002) Resazurin microtiter assay plate: simple and inexpensive method for detection of drug resistance in Mycobacterium tuberculosis. Antimicrob Agents Chemother. 46, 2720-2722
- 59. Patel, A. V., Turner, R. D., Rifflet, A., Acosta-Martin, A. E., Nichols, A., Awad, M. M., et al. (2021) PGFinder, a novel analysis pipeline for the consistent, reproducible, and high-resolution structural analysis of bacterial peptidoglycans. Elife 10. https://doi.org/10.7554/eLife.70597
- 60. Rady, B. J., and Mesnage, S. (2024) PGFinder, an open-source software for peptidoglycomics: the structural analysis of bacterial peptidoglycan by LC-MS. Methods Mol. Biol. 2836, 111-132
- 61. Li, M., Muller, C., Frohlich, K., Gorka, O., Zhang, L., Gross, O., et al. (2019) Detection and characterization of a mycobacterial L-Arabinofuranose ABC transporter identified with a rapid lipoproteomics protocol. Cell Chem. Biol. 26, 852-862.e856
- 62. Cox, J., and Mann, M. (2008) MaxQuant enables high peptide identification rates, individualized p.p.b.-range mass accuracies and proteomewide protein quantification. Nat. Biotechnol. 26, 1367-1372
- 63. Tyanova, S., Temu, T., and Cox, J. (2016) The MaxQuant computational platform for mass spectrometry-based shotgun proteomics. Nat. Protoc. 11, 2301-2319
- 64. Kapopoulou, A., Lew, J. M., and Cole, S. T. (2011) The MycoBrowser portal: a comprehensive and manually annotated resource for mycobacterial genomes. Tuberculosis (Edinb) 91, 8-13

